

03,09

The influence of samarium impurity defects on the luminescent and photocatalytic properties of titanium dioxide nanoparticles

© I.V. Egelskii^{1,2}, M.A. Pugachevskii¹

¹ South-West State University,
Kursk, Russia

² Moscow Institute of Physics and Technology (National Research University),
Dolgoprudny, Moscow Region, Russia

E-mail: ive1996@yandex.ru

Received December 28, 2024

Revised March 11, 2025

Accepted March 13, 2025

Nanoparticles of titanium dioxide doped with the rare-earth element samarium were synthesized using the hydrothermal method. The synthesized particles were characterized using transmission and scanning electron microscopy, Fourier-transform infrared spectroscopy, and X-ray diffraction. The bandgap of the obtained nanomaterials was determined based on the results of diffuse reflectance spectroscopy. The photoluminescent properties of the doped titanium dioxide particles were investigated at an optical excitation wavelength of 473 nm. The photocatalytic activity of the particles was studied in the degradation reaction of methylene blue in an aqueous solution under ultraviolet irradiation. The samarium-doped titanium dioxide nanoparticles exhibited enhanced photocatalytic activity compared to the undoped sample. The increased activity of the particles is attributed to the formation of additional energy levels within the bandgap due to impurity-induced defects, which leads to a reduction in the recombination probability of charge carriers generated during the photocatalytic process. The results obtained in this study demonstrate the potential application of samarium-doped titanium dioxide nanoparticles in photocatalytic applications, particularly for the removal of organic pollutants from aqueous environments.

Keywords: nanoparticles, titanium dioxide, samarium doping, hydrothermal synthesis, photoluminescence, photocatalysis.

DOI: 10.61011/PSS.2025.03.60872.357

1. Introduction

Titanium dioxide (TiO₂) is a semiconductor wide-band material with unique physical and chemical properties, which provide for its active use in various fields, such as biomedicine, photovoltaics, environmental applications, including treatment of water and air media from organic pollutants etc. [1–3].

It is known that most popular polymorphous modifications of titanium dioxide are anatase, rutile and brookite [4]. In the context of photocatalytic applications, the highest efficacy is demonstrated by pure anatase or its mixture of rutile. However, at heating above 400 °C an irreversible phase transition of anatase to rutile is observed [5].

Hydrothermal synthesis is a well-controlled method making it possible to produce nanoparticles of transition metal oxides with the specified elemental composition and narrow size distribution [6–8]. Besides, this process is easily implementable, reproducible and inexpensive [9–12].

It is important to note that the characteristics and properties of the produced titanium dioxide nanoparticles are also affected by the used methods of purification from organic compounds that arise in process of synthesis. The studies show that the selection of temperature modes for the hydrothermal method and use of different solvents

may substantially impact the structure of TiO₂ [5,13,14]. Besides, for the low-temperature synthesis the important stage of nanoparticle purification is annealing, which may cause size changes and modification of the band gap, which determine photoluminescent and photocatalytic properties of the materials [15–17].

Doping (alloying) of titanium dioxide is actively used to improve its photocatalytic and optical properties [18–24]. In this case the impurity defects, due to formation of additional energy levels, may both result in the change of the band gap width and formation of the charge traps. Thus, in particular, the addition of rare earth element samarium (Sm) to TiO₂ causes reduction in the particle size and formation of charge carrier traps by ions Sm³⁺, which are the key reasons making it possible to moderate the recombination of electron-hole pairs and, accordingly, improve the photocatalytic properties [25–29]. Besides, doping of titanium dioxide with impurity elements may promote improvement of its thermodynamic stability, which will make it possible to expand its use in high-temperature applications [30].

The objective of this paper is to identify the quantitative patterns in the effect of impurity rare earth element Sm at optic and photochemical properties of titanium dioxide nanoparticles, synthesized by hydrothermal method.

2. Experimental procedures

Hydrothermal synthesis of titanium dioxide nanoparticles was carried out in an autoclave reactor OLT-PH Xiamen Ollital Technology with teflon insert with volume of 30 ml. For this purpose, isopropanol (C_3H_8O) and samarium hydrate nitrate ($Sm(NO_3)_3 \cdot 6H_2O$) were added to titanium tetrabutoxide (IV) ($Ti(C_4H_9O)_4$), and then the produced mix was mixed using a magnetic mixer at 1000 revs/min. Then distilled water (H_2O) was added in drops to the system. The end content was gradually heated in a closed autoclave from 20 ± 5 to 120 ± 5 °C with speed of 4 °C per minute, and then the substance was soaked in the autoclave at constant temperature for 24 hours. The produced material was washed by hexane (C_6H_{14}) under continuous mixing with a magnetic mixer, and then centrifuged for solid phase deposition. The specimens were dried at room temperature to form dry powder of titanium dioxide doped with samarium. Further the synthesized particles were exposed to thermal annealing at temperature 500 °C.

Chemical composition of the specimens was determined using infrared Fourier transform spectrometer Nicolet iS50 (measurements in the range — 50–15 000 cm^{-1} , spectral resolution — 0.125 cm^{-1}). Morphological characteristics and particle-size composition of titanium dioxide (TiO_2) were studied using scanning electron microscope JSM-6610LV (spatial resolution: in high vacuum mode — 3.0 nm (30 kV), in low vacuum mode — 4.0 nm (30 kV), accelerating voltage: 0.3–30 kV, magnification range: $\times 5$ – $\times 300\,000$, tungsten cathode), equipped with energy-dispersive spectrometric detector X-Max by Oxford Instruments (energy range of X-ray radiation: 7 keV–11 MeV, guaranteed resolution by energy in lines: MnK_α — 127 eV, CK_α — 56 eV), and also transmission electron microscope JEOL JEM-2100 (accelerating voltage — 200 kV, spatial resolution — 1.9 Å, magnification range — from $\times 50$ to $\times 1\,500\,000$). Phase composition of nanoparticles was defined using the method of X-ray diffractometry at installation GBC EMMA (radiation capacity — 2.2 kW, spot size — 12 mm, minimum pitch of goniometer — 0.02°, goniometer radius — 180–250 mm, rotation range — 30–160°). Optical properties of specimens were studied by the method of diffuse reflectance spectroscopy (DRS) at spectrophotometer Perkin Elmer Lambda 950 (wavelength range 180 nm–10 μm ; monochromators with a holographic grating 1440 lines/mm (UV/View); 360 lines/mm (BIK); resolution ≤ 0.05 nm (UV/View), ≤ 0.20 nm (BIK); reproducibility of wavelength ± 0.005 nm (UV/View), ± 0.02 nm (BIK)). Photoluminescent properties were analyzed using the method of laser combination 3D-microspectroscopy Nanofinder 30 (radiation wavelength — 473 nm, radiation capacity — 2.62 mW, exposure time — 30 s, spectral resolution — 0.8 cm^{-1} , spatial resolution — 0.5 μm).

The paper synthesized four specimens of TiO_2 with different atomic share of Sm relative to Ti (0.4, 0.8, 1 and 1.6 at.%), and also a specimen of titanium dioxide without addition of impurities, with the purpose of their

comparative complex analysis. The studied nanoparticles were dispersed in distilled water for 30 minutes. The photochemical properties of the synthesized specimens were studied using the example of the reaction of catalytic degradation of organic dye — methylene blue (MB) when radiated with a source of ultraviolet light at intensity 6.3 W/m². Detection of residual content of MB in a cuvette in process of photocatalytic reaction in the presence of TiO_2 nanoparticles with different content of Sm was carried out using spectrophotometer SF-2000 (spectral range of measurements 190–1000 nm, spectral resolution 1 nm). Optical density of the solution was measured at wavelength 664 nm within the specified intervals of radiation time for 60 minutes.

3. Findings and their discussion

Data of IR Fourier spectroscopy showed that washing and subsequent annealing of hydrothermal synthesis products in a furnace make it possible to significantly reduce the content of residual carbon-containing compounds in their chemical composition. Using elemental analysis, the atomic mass of samarium was determined in respect to titanium, which is reflected in the designation of specimens: $TiO_2:Sm-0.4\%$, $TiO_2:Sm-0.8\%$, $TiO_2:Sm-1\%$, $TiO_2:Sm-1.6\%$. According to the results of the transmission electron microscopy, the annealed nanoparticles, both without an impurity (Figure 1, *a*) and doped with samarium (Figure 1, *b*), had tetragonal shape with rounded tops.

Following the results of particle-size composition, it was determined that the average size of individual particles of TiO_2 without impurities was 12 ± 2 nm (Figure 2, *a*), while nanoparticles doped with samarium 0.4% had size of 11 ± 2 nm (Figure 2, *b*). The reduction of doped particles size may be explained by the growth of the number of TiO_2 particle crystallization centers in the reaction mix with the increased content of samarium. Besides, the presence of impurities in the particles slows down the speed of their growth upon annealing as a result of diffusion Smith–Zener braking [31].

The phase composition of the specimens was characterized by the method of X-ray diffractometry. According to the obtained results (see Figure 3), in the range of angles 2θ from 20 to 70° the diffraction peaks are identified, the interplanar spacings of which correspond to 3.51 Å [101]; 2.36 Å [004]; 1.89 Å [200]; 1.69 Å [105]; 1.47 Å [213], which matches maps 1 — 562, 2 — 387 of ASTM database [32]. These interplanar spacings were detected both for TiO_2 without impurities and for TiO_2 doped with samarium with content from 0.4 to 1.6%. However, it should be noted, that as the percentage content of samarium in the specimens increased, the intensity of X-ray peaks decreased, and no additional reflexes were observed in diffraction patterns.

The average size of the coherent scattering region (CSR) for TiO_2 nanoparticles without doping calculated using Debye–Scherrer formula, was 12 ± 0.5 nm. Specimens

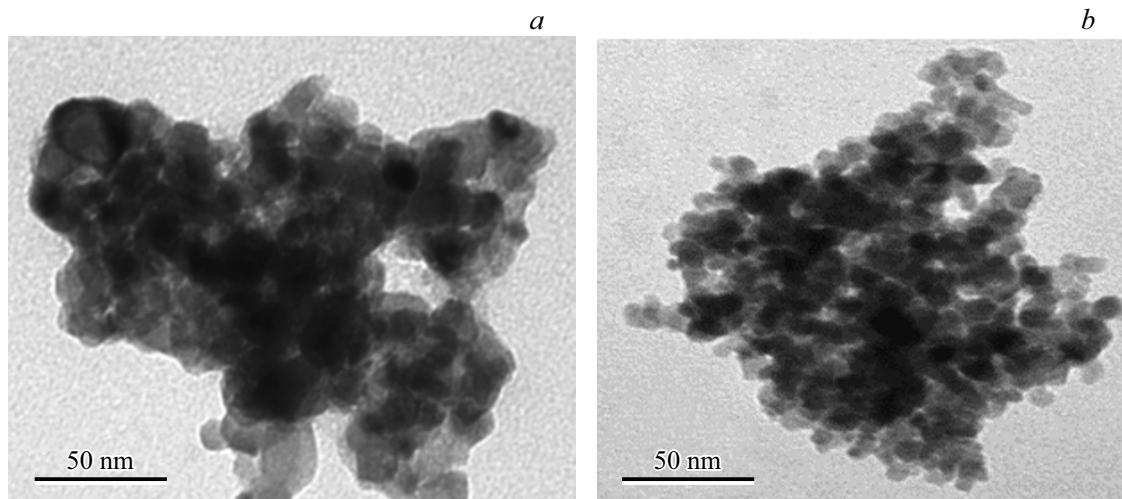


Figure 1. Images of transmission electron microscopy: *a* — TiO_2 ; *b* — $\text{TiO}_2:\text{Sm}-0.4\%$.

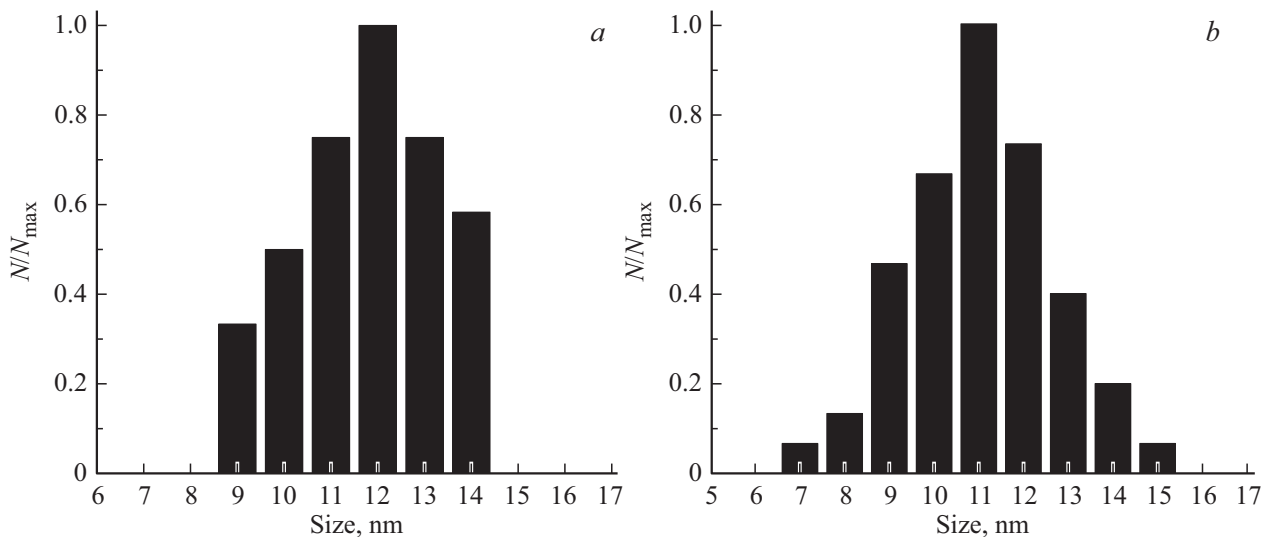


Figure 2. Particle-size composition of titanium dioxide nanoparticles: *a* — TiO_2 without impurities; *b* — $\text{TiO}_2:\text{Sm}-0.4\%$.

with impurities of Sm were characterized by CSR dimensions from 8 ± 0.5 to 6 ± 0.5 nm, decreasing with the increase of the percentage content of impurity.

To characterize the electron structure of synthesized specimens, optical properties of doped TiO_2 nanoparticles were studied. For this purpose, diffuse reflectance spectroscopy of specimens was performed, the results of which using the example of $\text{TiO}_2:\text{Sm}-0.4\%$ were given in Figure 4.

Using the reflectance spectrum converted with Kubelka–Munk function (1) into Tauc curve, the width of band gap E_g was defined.

$$F(R) = \frac{(1-R)^2}{2R}. \quad (1)$$

The band gap width was characterized both for direct (Figure 5, *a*) and indirect optical transitions (Figure 5, *b*), and made 3.16 ± 0.05 and 2.75 ± 0.05 eV, accordingly.

Previously we received data on E_g for TiO_2 nanoparticles without impurity [21], where it was shown that E_g takes values 3.21 ± 0.05 and 2.81 ± 0.05 eV for direct and indirect resolved transitions, respectively. From comparison of the results you may notice that doping of TiO_2 nanoparticles with samarium causes minor reduction of band gap width. This trend was noted at higher concentrations of samarium impurity, too.

To study the optical properties of titanium dioxide nanoparticles with various content of samarium, their photoluminescence (PL) spectra were also studied at excitation wavelength of 473 nm. The luminescent properties were studied in the wavelength range from 500 to 800 nm, where strong luminescent lines were detected, demonstrated in Figure 6.

For wavelength 473 nm (2.62 eV) of exciting radiation, transition $\text{Sm}^{3+} \ ^6H_{5/2} \rightarrow \ ^4I_{9/2}$ is possible. After excitation

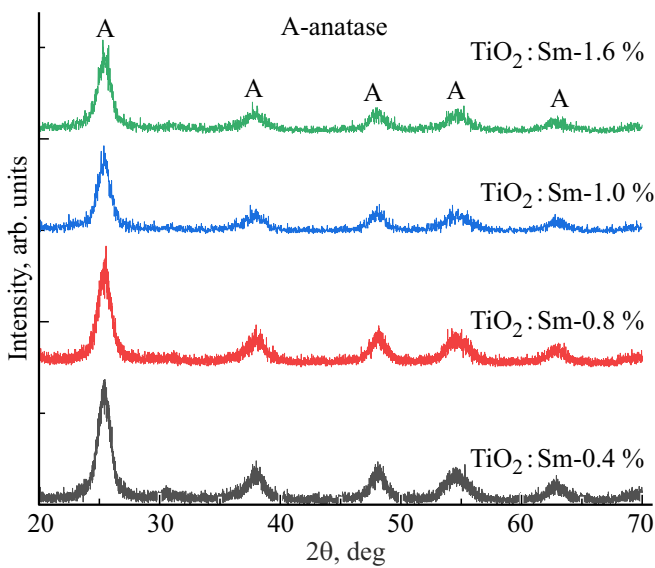


Figure 3. X-ray diffraction patterns of titanium dioxide nanoparticles doped with different concentrations of samarium.

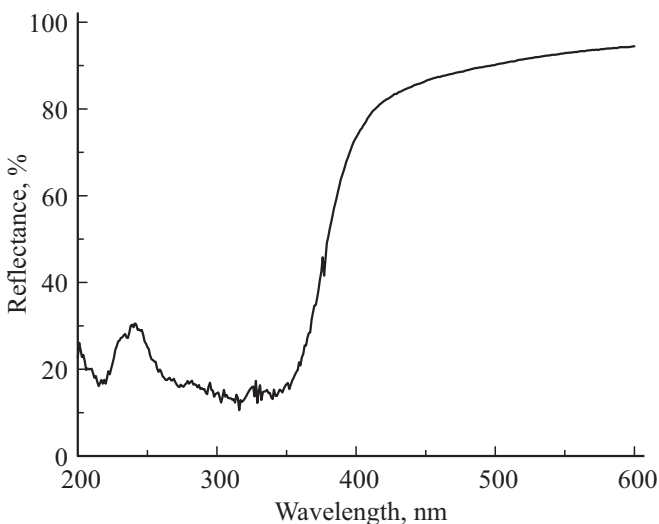


Figure 4. Spectrum of diffuse reflectance of samarium (0.4%) doped specimen of TiO_2 .

of level $^4I_{9/2}$, nonradiative relaxation happens to lower levels, such as $^4G_{5/2}$ (~ 2.2 eV), which is the main radiation state for Sm^{3+} . It was found that the detected luminescence peaks belong to Sm^{3+} : near 565 nm they are caused by transition $^4G_{5/2} \rightarrow ^6H_{5/2}$, near 600 nm — by transition $^4G_{5/2} \rightarrow ^7H_{7/2}$, 650 nm — $^4G_{5/2} \rightarrow ^7H_{9/2}$. Indirect excitation of ions Sm^{3+} is also possible via trap levels in the band gap of TiO_2 , related to oxygen vacancies. Oxygen vacancies in titanium dioxide may absorb photons 473 nm, creating electron-hole pairs, which in turn may participate in indirect excitation Sm^{3+} . According to the experiment results, as Sm concentration increased, the photoluminescence peak intensity decreased. Figure 7 schematically demonstrates the

possible processes of energy transitions, happening upon excitation with blue laser (473 nm) of TiO_2 nanoparticles doped with samarium.

Explaining the produced results, it may be noted that due to the presence of the Sm impurity in the electron structure of nanoparticles, traps were formed for the charge carriers, which due to the lower probability of reverse recombination may substantially increase the life time of excited electrons, and therefore cause photoluminescence of specimens. It is interesting that the highest photoluminescence is observed at concentration of Sm impurity 0.4%. As impurity content increases, the luminescence glow decreases substantially, which may be explained by the development of multiple structural defects around the impurity atoms, capable of causing strong quenching of PL due to nonradiative transitions. Concentration quenching of luminescence in the samarium-doped TiO_2 is possible at the expense of some interrelated mechanisms, such as tunneling, nonradiative relaxation, cross relaxation, and also clusterization Sm^{3+} , which are substantially activated at high concentration of Sm^{3+} ions. At high concentration of dopant, the distance between ions Sm^{3+} reduces, which facilitates the transfer of energy between them and improves the probability of nonradiative relaxation. Instead of photon radiation, the excitation energy scatters through nonradiative transitions, including via tunneling and scattering in phonons. Besides, high concentrations of dopant provoke aggregation of ions Sm^{3+} into clusters. These clusters damage the crystalline structure of TiO_2 , creating structural defects, which will also serve as luminescence quenching centers.

When Sm^{3+} is substituted in the crystalline lattice nodes, the charge compensation mechanism is implemented via decrease of energy barrier to form oxygen vacancies near Sm^{3+} . This must presumably result in more defects of titanium oxide TiO_2 ($x < 2$) and within the limit, at high concentration of dopant Sm, even to rearrangement of its structure to Ti_2O_3 . However, in the concentrations of Sm that we studied, the formation of Ti_2O_3 in the specimens on X-ray diffraction patterns was not recorded.

The studies of photodegradation of methylene blue (MB) dye in the process of photocatalytic reaction in presence of titanium dioxide nanoparticles, both impurity-free and doped with Sm, demonstrated that photochemical activity of TiO_2 nanoparticles doped with samarium with any percentage content is higher than without adding impurity (Figure 8).

For photocatalytic reaction, the speed constant k was measured:

$$C(t) = C_0 \exp[-kt]. \quad (2)$$

From formula (2) formula (3) proceeds:

$$k \approx -\ln\left(\frac{C}{C_0}\right) / t, \quad (3)$$

where C_0 and C is residual content of methylene blue dye in process of photocatalytic reaction at the initial and current moments of time, respectively.

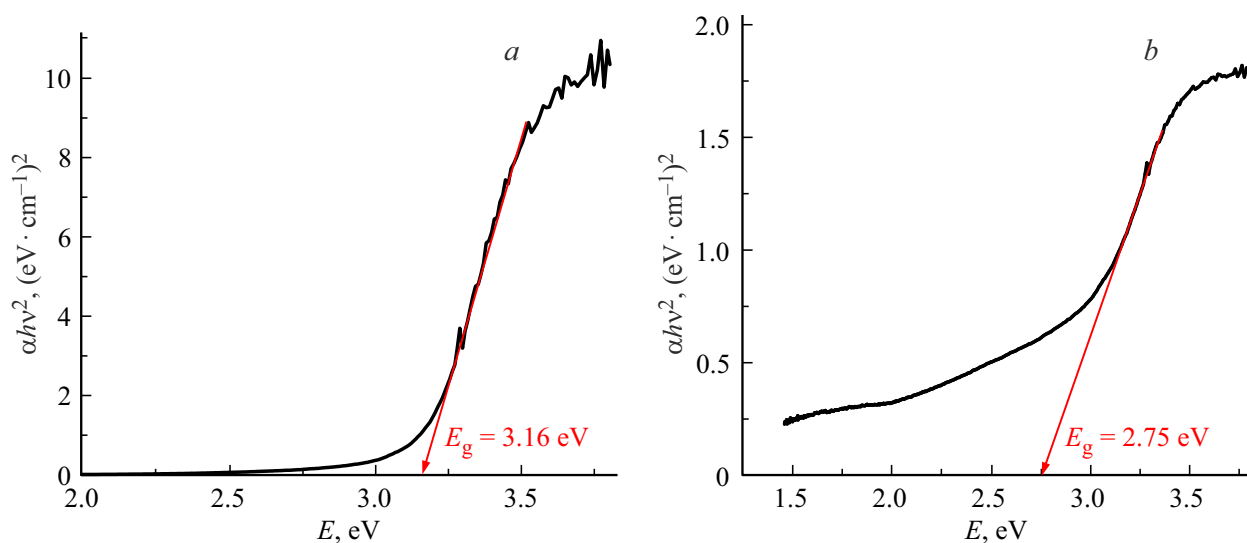


Figure 5. Definition of band gap of $\text{TiO}_2:\text{Sm}-0.4\%$ using Tauc curves: *a* — direct transition, *b* — indirect transition.

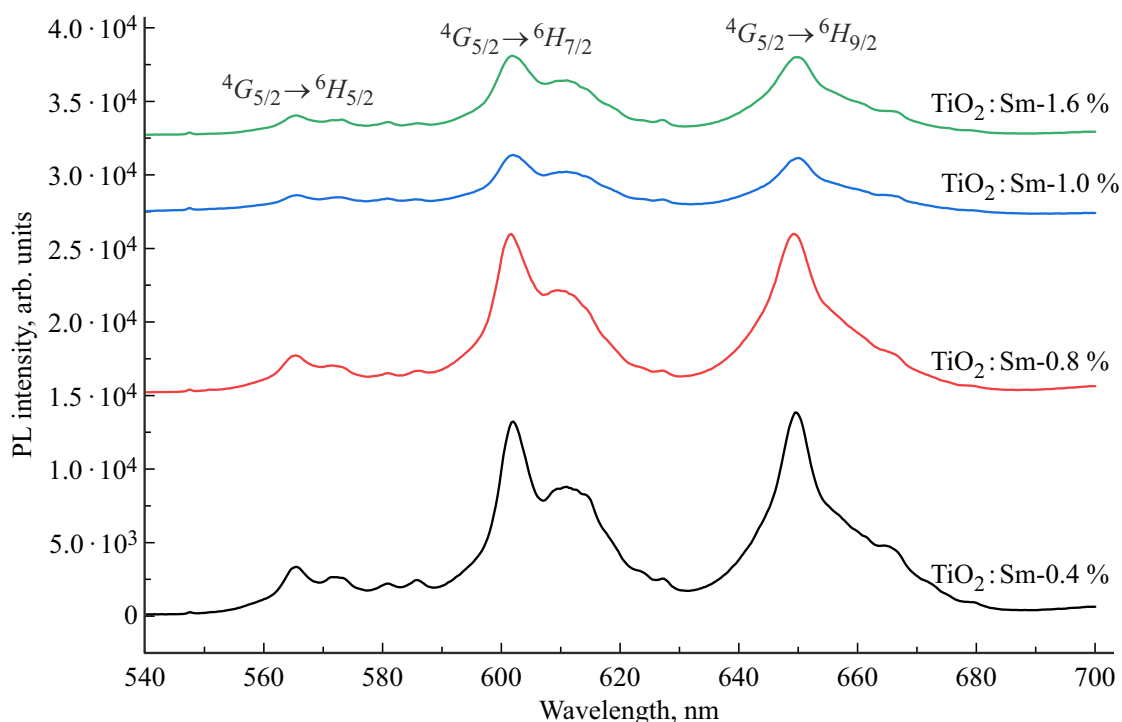


Figure 6. PL spectra of TiO_2 specimens doped with Sm ($\lambda_{\text{ex}} = 473 \text{ nm}$).

Constants of reaction speed of photocatalytic degradation of MB in presence of TiO_2 nanoparticles under ultraviolet radiation are presented in Figure 9. According to the obtained results, the highest photocatalytic activity is specific for TiO_2 nanoparticles with content of Sm impurity of 0.4%, in this case the constant of reaction speed k was $20.6 \cdot 10^{-3} \text{ min}^{-1}$, which is twice higher than for TiO_2 nanoparticles without impurity.

Therefore, it was found that samarium doping results in higher photocatalytic activity of titanium dioxide nanopar-

ticles. As noted previously, in this case impurity ions Sm^{3+} create additional energy levels inside a band gap, which may serve as traps for the charge carriers, increasing their life time. This is confirmed by results of studies of the photoluminescent properties (see Figure 6), when at excitation wavelength 473 nm the photoluminescence glow is detected, which is specific for intrashell transitions of 4f-electrons. In photocatalytic process the excited charge carriers may migrate to the surface of the particles, where they launch a cascade of oxidation-reduction reactions to

produce active radicals, such as superoxide anion, hydroxyl radical, hydroperoxyl radical etc. These forms of radicals are the active component of the photocatalytic process, directly attacking organic compounds and causing their

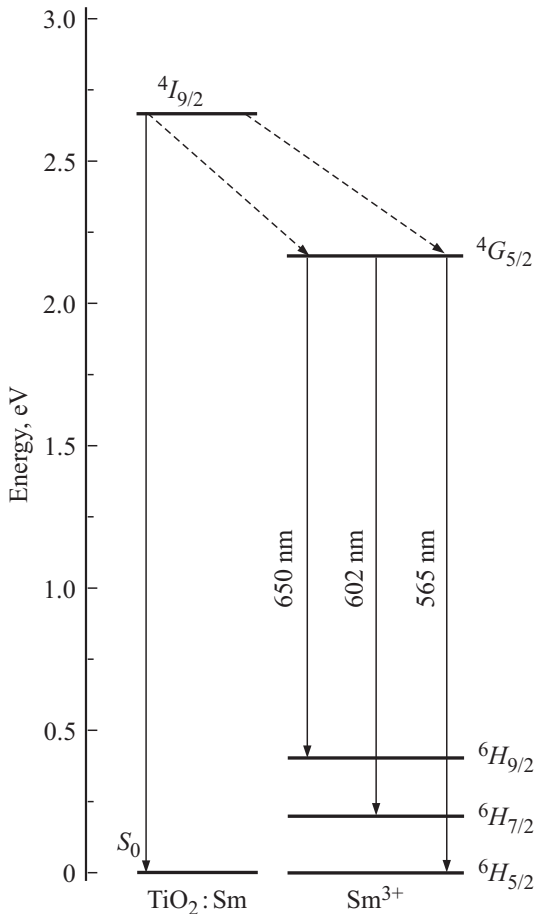


Figure 7. Diagram of energy transfer as a result of radiation of Sm-doped specimens ($\lambda_{\text{ex}} = 473 \text{ nm}$).

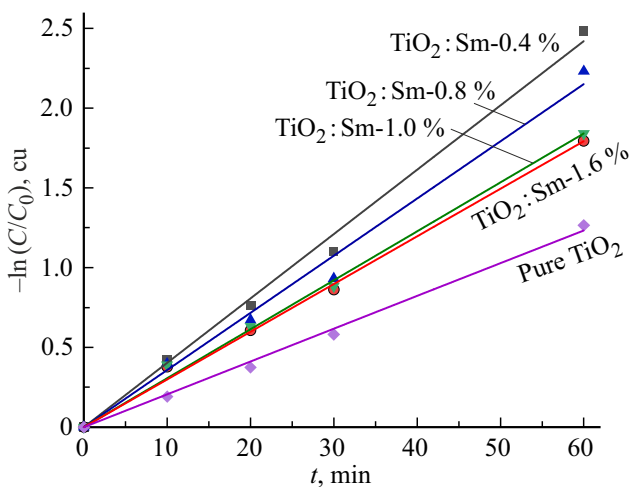


Figure 8. Photocatalytic degradation of MB under UV-radiation in presence of TiO_2 nanoparticles with different concentration of Sm.

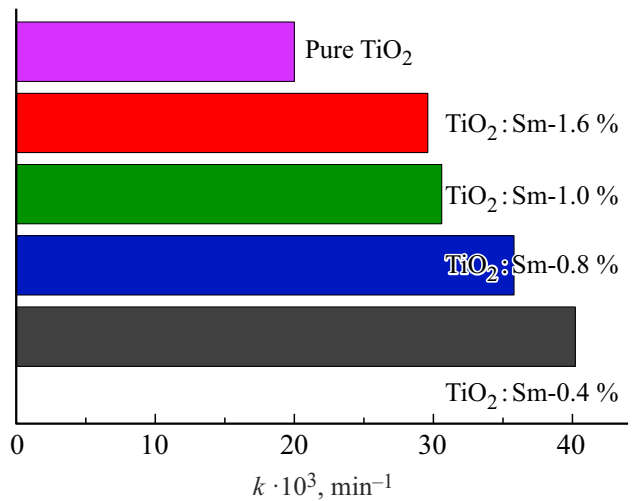


Figure 9. Constants of reaction speed of photocatalytic degradation of MB under UV-radiation at different concentration of Sm in TiO_2 .

decomposition. As you can see from the obtained results, the best efficacy of the photocatalytic process is achieved when TiO_2 nanoparticles are doped with samarium at concentration of 0.4%. However, at higher content of samarium, photocatalytic activity of TiO_2 nanoparticles decreases, which may be related to drastic increase of the number of structural defects in the doped particles. These defects introduce already negative contribution to the activity of the particles, since on the one hand they may cause nonradiative recombination, including Auger recombination, of the excited charge carriers, and on the other hand, they substantially decrease the probability of charge release to the surface and, accordingly, prevent formation of active chemical radicals in the photocatalytic system [33].

Summing up the above, you may nevertheless note that the results obtained in the paper demonstrate the prospect of using samarium-doped titanium dioxide nanoparticles in photocatalysis. Thus, one of the important applied uses of synthesized particles may be photocatalytic treatment of water and air media from organic pollutants.

4. Conclusions

The hydrothermal method synthesized titanium dioxide nanoparticles doped with samarium having concentrations of 0.4, 0.8, 1 and 1.6%. As a result of phase analysis, it was established that nanoparticles have the anatase type structure. The studies of the transmission electron microscopy and X-ray diffraction analysis demonstrated that doping of TiO_2 nanoparticles with samarium causes decrease of their average size. According to the results of diffuse reflectance spectroscopy, the width of $\text{TiO}_2:\text{Sm}-0.4\%$ band gap is 3.16 and 2.75 eV for direct and indirect resolved transitions, respectively. Photoluminescence spectra arising due to

intrashell transitions of $4f$ -electrons indicate lower intensity of PL with the increase of samarium content in the specimens. It was established that the constant of photocatalytic reaction speed for $\text{TiO}_2:\text{Sm}-0.4\%$ nanoparticles is twice higher than for the TiO_2 nanoparticles without impurity, which indicates that titanium dioxide nanoparticles doping with samarium improves their photocatalytic properties. However, high concentration of Sm causes formation of considerable number of structural defects, providing for nonradiative recombination of excited charge carriers and preventing their exit to the surface. The results obtained in the paper demonstrate the prospects of samarium-doped titanium dioxide nanoparticles for photocatalytic applications.

Funding

This study was funded by the Ministry of Science and Higher Education of the Russian Federation (contract No. 075-03-2025-526).

Conflict of interest

The authors declare that they have no conflict of interest.

References

- [1] K.P. Gopinath, N.V. Madhav, A. Krishnan, R. Malolan, G. Rangarajan. *J. Environ. Manage* **270**, 110906 (2020).
- [2] D. Ziental, B. Czarczynska-Goslinska, D.T. Mlynarczyk, A. Glowacka-Sobotta, B. Stanisz, T. Goslinski, L. Sobotta. *Nanomaterials* **10**, 2, 387 (2020).
- [3] A. Hashemi Monfared, M. Jamshidi. *Prog. Org. Coatings* **136** (2019).
- [4] M.K. Singh, M.S. Mehata. *Optik (Stuttg)* **193**, 163011 (2019).
- [5] R.S. Dubey. *Mater. Lett.* **215**, 312–317 (2018).
- [6] Y.V. Kolen'ko, B.R. Churagulov, M. Kunst, L. Mazerolles, C. Colbeau-Justin. *Appl. Catal. B: Environ.* **54**, 1, 51–58 (2004).
- [7] H. Schmidt. *Appl. Organomet. Chem.* **15**, 5, 331–343 (2001).
- [8] R.S. Dubey, K.V. Krishnamurthy, S. Singh. *Results Phys.* **14**, 102390 (2019).
- [9] C.H. Zhou, S. Xu, Y. Yang, B.C. Yang, H. Hu, Z.C. Quan, B. Sebo, B.L. Chen, Q.D. Tai, Z.H. Sun, X.Z. Zhao. *Electrochim. Acta* **56**, 11, 4308–4314 (2011).
- [10] G.K. Sendil, E. Soundarrajan, M.R. Ranjitha, R.A. Klaivani, S. Raghu. *Asian J. Chem.* **35**, 1, 45–51 (2023).
- [11] N. Kumar, S.N. Hazarika, S. Limbu, R. Boruah, P. Deb, N.D. Namsa, S.K. Das. *Micropor. Mesopor. Mat.* **213** (2015).
- [12] V.V. Zlobin, V.N. Nevedomskiy, O.V. Almjashaeva. *Mater. Today Commun.* **36**, 106436 (2023).
- [13] M. Zhang, T. Chen, Y. Wang. *RSC Adv.* **7**, 83, 52755–52761 (2017).
- [14] V. Serga, R. Burve, A. Krumina, V. Pankratova, A.I. Popov, V. Pankratov. *J. Mater. Res. Technol.* **13**, 2350–2360 (2021).
- [15] B. Bulut, Ş. Duman. *Konya J. Eng. Sci.* **9**, 3, 676–685 (2021).
- [16] K. Mushtaq, M. Saeed, W. Gul, M. Munir, A. Firdous, T. Yousaf, K. Khan, H.M.R. Sarwar, M.A. Riaz, S. Zahid. *Inorg. Nano-Met. Chem.* **50**, 7, 580–586 (2020).
- [17] J. Moma, J. Baloyi. *IntechOpen* 79374 (2019).
- [18] L. Zhou, M. Xie, C. Rao, H. Su, Y. Pang, H. Lou, D. Yang, X. Qiu. *Chem. Eng. J.* **471**, 144574 (2023).
- [19] N.R. Khalid, E. Ahmed, A. Rasheed, M. Ahmad, M. Ramzan, A. Shakoor, A. Elahi, S.M. Abbas, R. Hussain, N.A. Niaz. *J. Ovonic Res.* **11**, 5, 107–112 (2015).
- [20] P. Rajput, M.P. Deshpande, H.R. Bhoi, N.M. Suchak, P.H. Desai, S.H. Chaki, S.J. Pandya, M. Mishra, S.V. Bhatt, D.K. Tiwari, V. Sathe. *Chem. Phys. Impact* **5**, 100101 (2022).
- [21] Yu.A. Egelskii, I.V. Pugachevskii, M.A. Martynova, E.A. Neruchev. *Izvestiya YuZGU. Ser. Tekhnika i Tekhnologii* **14**, 2, 108–121 (2024) (in Russian).
- [22] M. Murayama, K. Yoda, K. Shiraishi, S. Guan, S. Komuro, X. Zhao. *Opt. Photonics J.* **8**, 5, 85014 (2018).
- [23] E. Radha, D. Komaraiah, R. Sayanna, J. Sivakumar. *J. Lumin.* **244**, 118727 (2022).
- [24] A. Kutuzova, J.O. Moritz, N.G. Moustakas, T. Dontsova, T. Peppel, J. Strunk. *Appl. Nanosci.* **13**, 10, 6951–6966 (2023).
- [25] D. Ravikumar, S.C. Jeyakumar, S.S.J. Dhas, C.S. Biju, A. Sivakumar, R.S. Kumar, A.I. Almansour. *Mater. Sci. Semicond. Process* **173**, 108125 (2024).
- [26] A. Ishizawa, H. Aizawa, H. Isshiki, S. Kaku, K. Miyano, X. Zhao, M. Murayama. *Jpn. J. Appl. Phys.* **63**, 3 (2024).
- [27] I. Apostolova, A. Apostolov, J. Wesselinowa. *Nanomaterials* **13**, 1, 13010145 (2023).
- [28] S. Ahmetović, Z. Vasiljević, V. Rajić, D. Bartolić, M. Novaković, N.B. Tadić, N. Cvjetičanin, M.V. Nikolić. *J. Alloys Compd.* **930**, 167423 (2023).
- [29] J. Li, B. Chu, Z. Xie, Y. Deng, Y. Zhou, L. Dong, B. Li, Z. Chen. *Catal. Lett.* **152**, 2, 489–502 (2022).
- [30] M.A. Pugachevskii, *Pisma V ZhTF* **38**, 7, 56–63 (2012) (in Russian).
- [31] M. Miodownik, E.A. Holm, G.N. Hassold. *Scr. Mater.* **42**, 12, 1173–1177 (2000).
- [32] Powder Diffraction File, Joint Committee on Powder Diffraction Standards, ASTM, Philadelphia, PA, 1967, Card 1 — 562, Card 2 — 387.
- [33] M.A. Pugachevskii, D.S. Rasseko, V.A. Stupin, N.E. Manturova, E.B. Artyushkova, E.V. Silina. *J. Mol. Liq.* **404**, 124946 (2024).

Translated by M.Verenikina